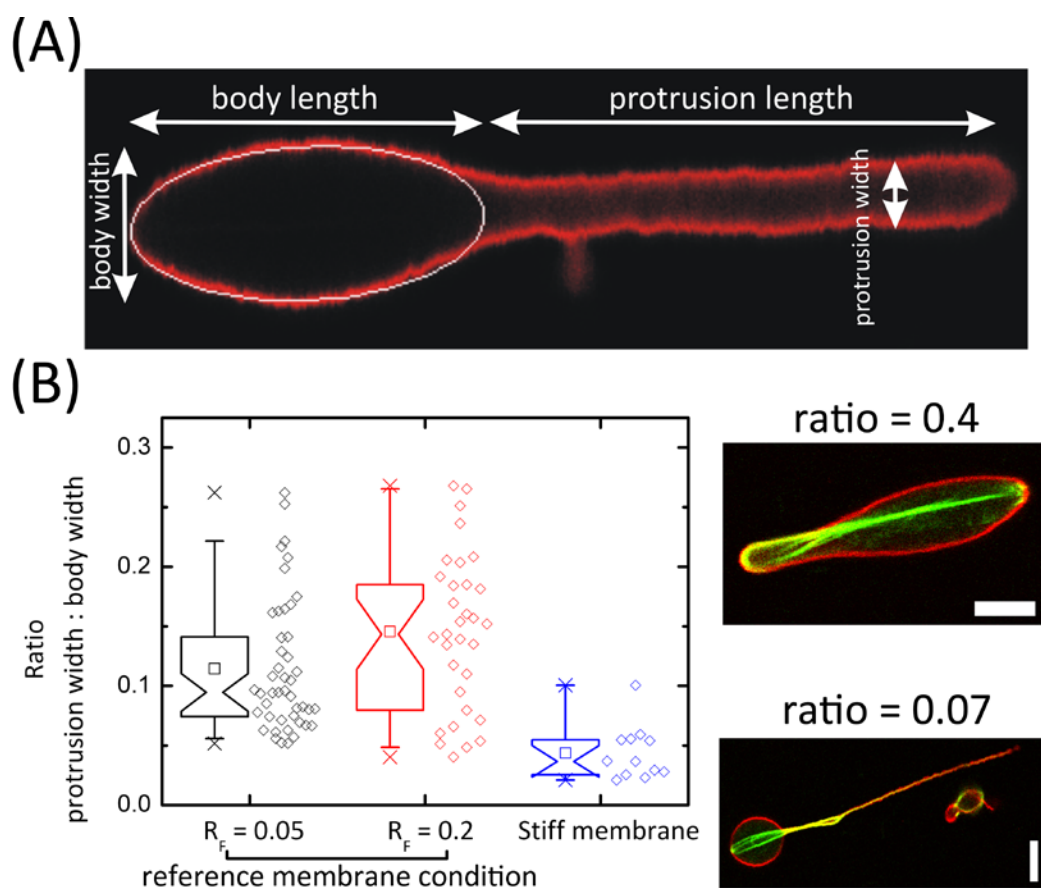
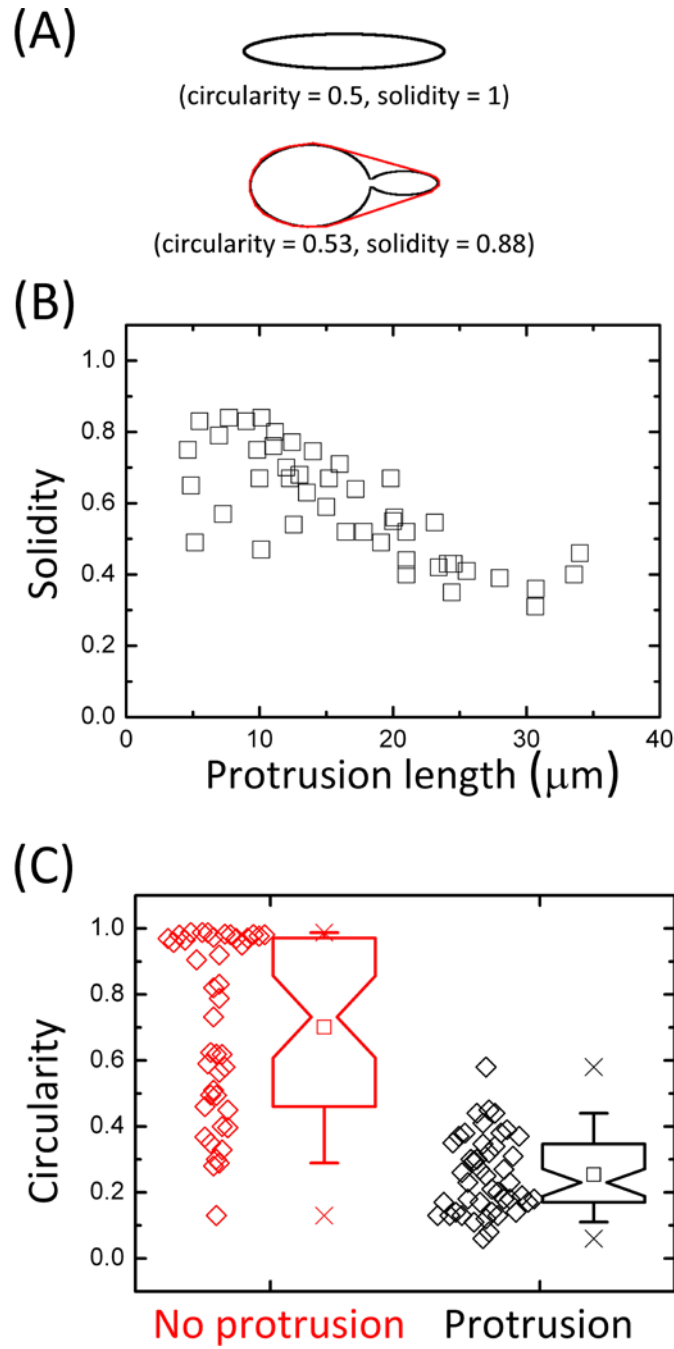


## Supplementary Material



**FIGURE S1** (A) Confocal image of a deformed liposome in which the white ellipse presents the result of fitting its main body contour to an ellipse and the white arrows indicate the lengths and widths of the body and the protrusion. (B) *Left*: Distributions of protrusion-to-body width ratios observed for actin-filled liposomes prepared under different conditions as labeled. Note that only liposomes having a protrusion-to-body width ratio below 0.3 are classified as “*protruded liposomes*” and are shown here. Liposome population sizes from left to right: 45, 32 and 12. *Right*: Confocal fluorescence images show a liposome classified as having no protrusion (*top panel*, protrusion-to-body width ratio = 0.4) and a liposome classified as having a protrusion (*bottom panel*, protrusion-to-body width ratio = 0.07). Red: membrane, green: actin. Scale bars: 5  $\mu\text{m}$ .



**FIGURE S2** Morphological characterization of liposomes encapsulating actin-fascin bundles at  $R_F = 0.05$ . (A) *Top*: circularity quantifies the deviation of a liposome shape from a circle. *Bottom*: solidity quantifies the degree of concavity of a liposome shape by comparing its area to that of a convex hull enclosing the shape, shown by the red line. Solidity and circularity range from 1 (for a circle) to 0. (B) The liposome solidity is inversely correlated with the protrusion length (correlation coefficient = -0.772,  $p < 0.001$ ). (C) Comparison of circularities of liposomes with (45 liposomes) and without (42 liposomes) protrusions.

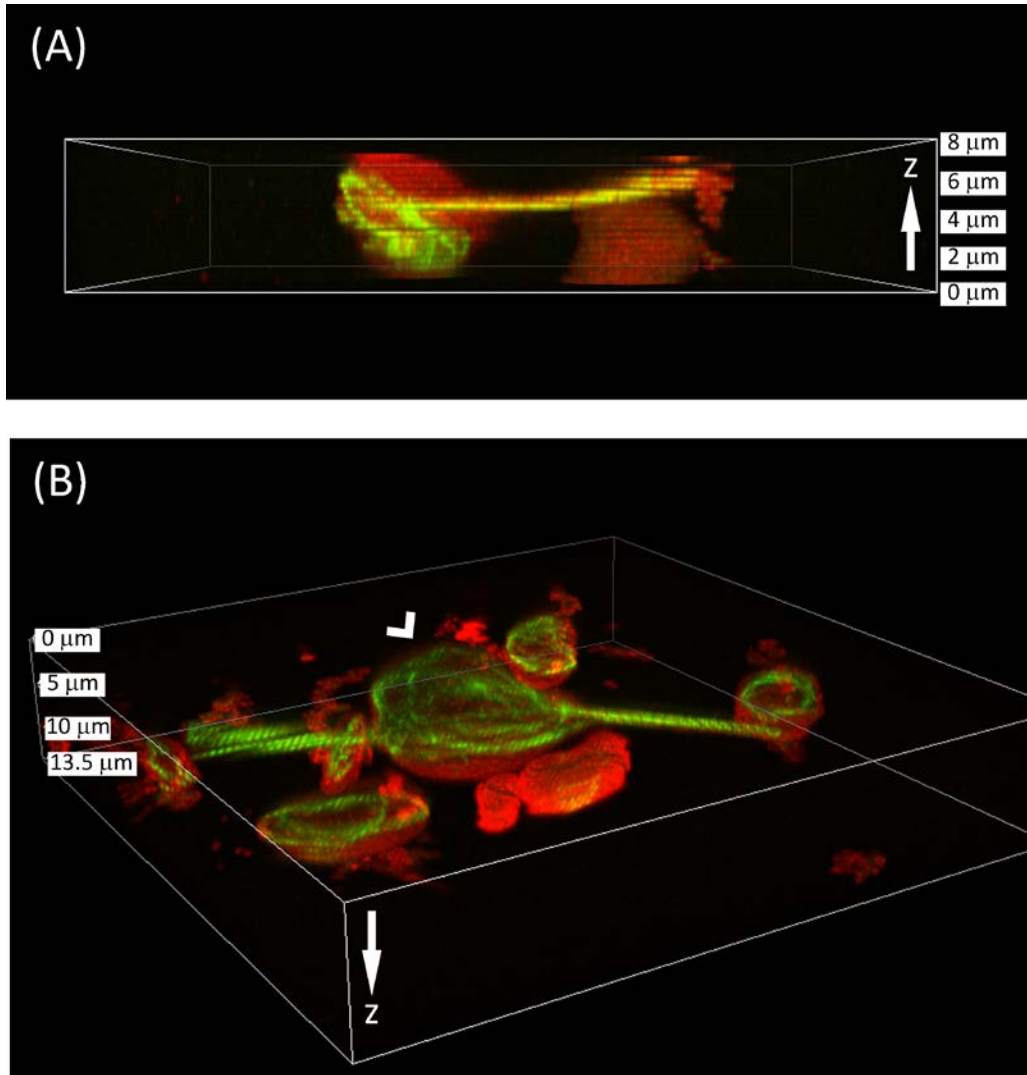


**FIGURE S3** 3D reconstructions of confocal fluorescence z-stacks obtained for liposomes encapsulating actin-fascin bundles. (A) A planar ring-like actin bundle structure in a protruded liposome. (B) Multiple ring-like structures of actin bundles (indicated by the white arrow head) inside a protruded liposome with two protrusions. Liposomes were formed at the *reference membrane* condition and with  $R_F = 0.05$ . Note that the smaller structures around the liposome are small liposomes. Red: membrane, green: actin.

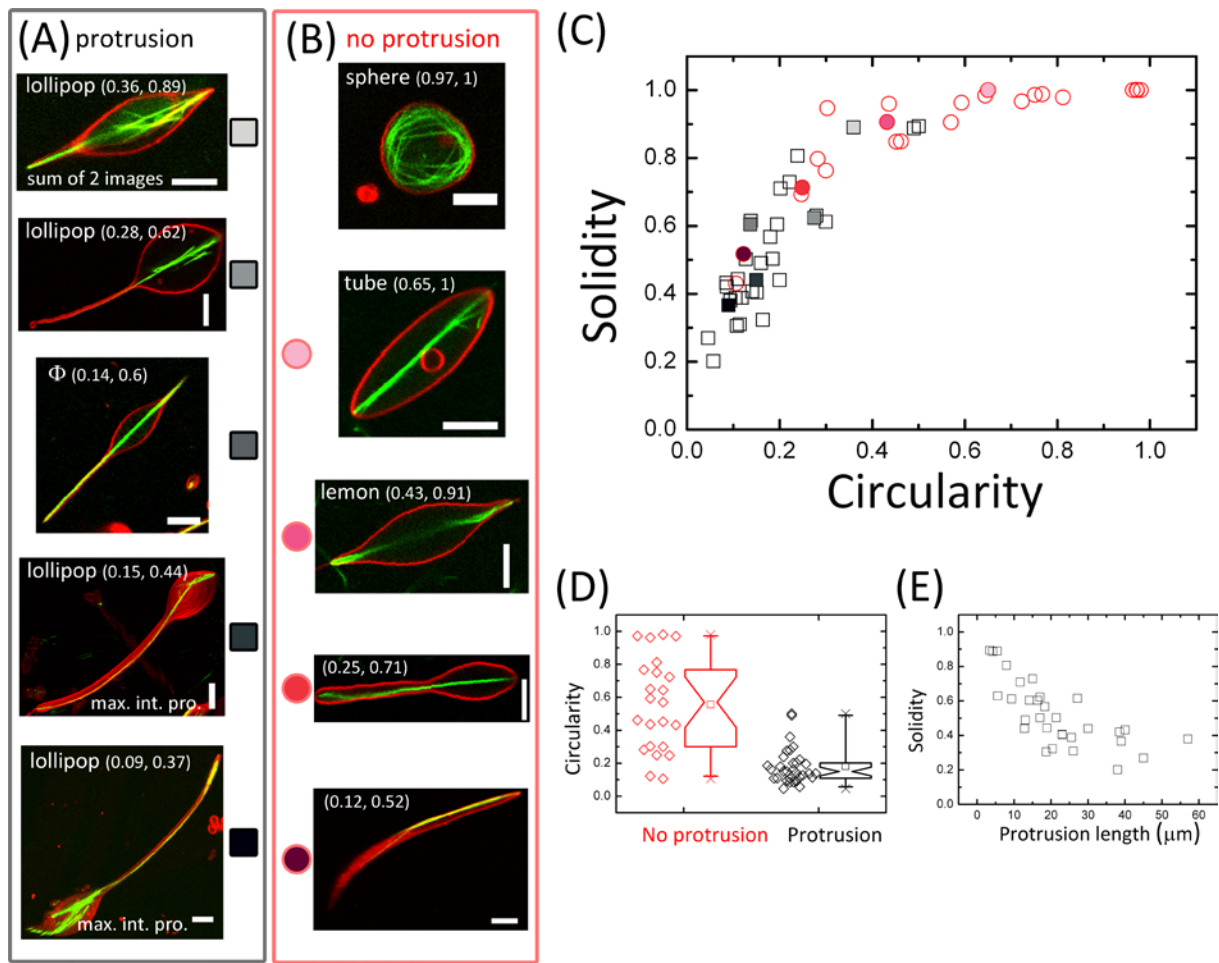
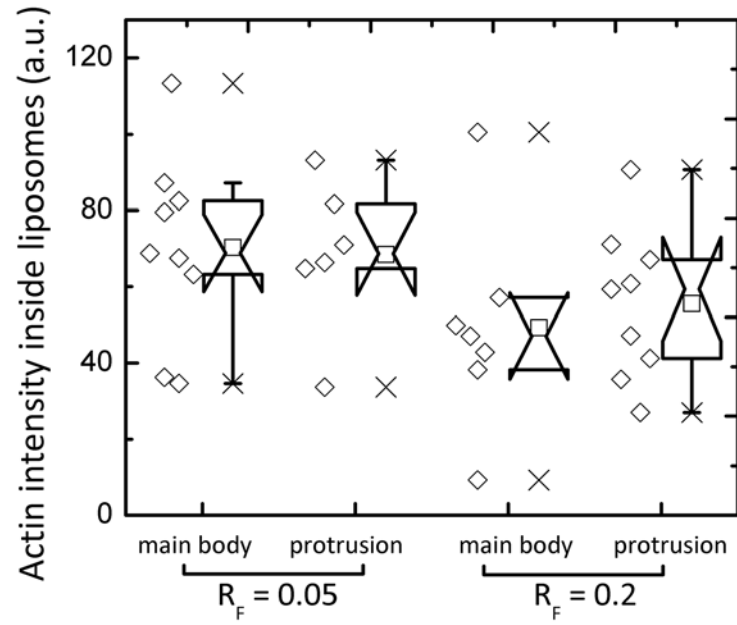


**FIGURE S4** Morphological characterization of a population of 55 liposomes encapsulating stiff actin-fascin bundles ( $R_F = 0.2$ ). (A and B) Confocal images of liposomes that are increasingly deformed (*top to bottom*). Images are single confocal sections recorded at the equatorial plane of the liposomes, except for the lollipop (0.36, 0.89), where 2 confocal images are summed to show the entire shape (*sum of 2 images*), and for the lollipop (0.15, 0.44) and (0.09, 0.37), where maximum intensity projections (*max. int. pro.*) are shown composed of  $p$  planes over a total  $z$ -range ( $z$  in  $\mu\text{m}$ ) of ( $p = 21$ ,  $z = 10$ ) and ( $p = 22$ ,  $z = 10.5$ ), respectively. Red: membrane, green: actin. Scale bars: 5  $\mu\text{m}$ . (C) The broad range of liposome shapes can be summarized in terms of circularity and solidity. Reddish symbols represent liposomes having no protrusion (23 liposomes) and black/grayish symbols represent liposomes with one or more protrusions (32 liposomes). Color-coded solid symbols correspond to images of liposomes in (A) and (B). (D) Circularities of liposomes with and without protrusions. Similar to the liposomes formed at low  $R_F$ , protruded liposomes have a lower circularity than most non-protruded liposomes. (E) The solidity is inversely correlated with the protrusion length (correlation coefficient = -0.724,  $p < 0.001$ ).

(A)



(B)

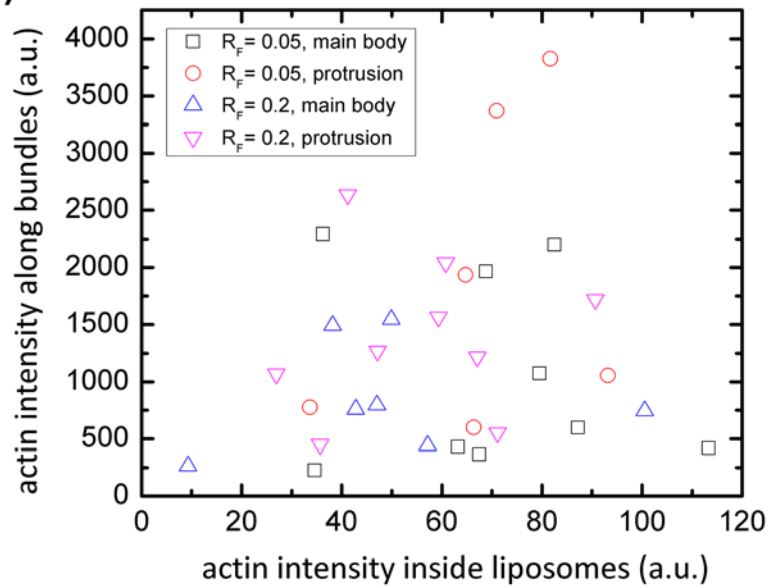


**FIGURE S5** (A) Fluorescence intensity of unbundled actin inside liposomes. Liposome population sizes from *left to right*: 9, 6, 7, 9. (B) There is no correlation between the fluorescence intensities of actin bundles and of unbundled actin in each liposome (correlation coefficient = 0.1258,  $p = 0.5001$ ).

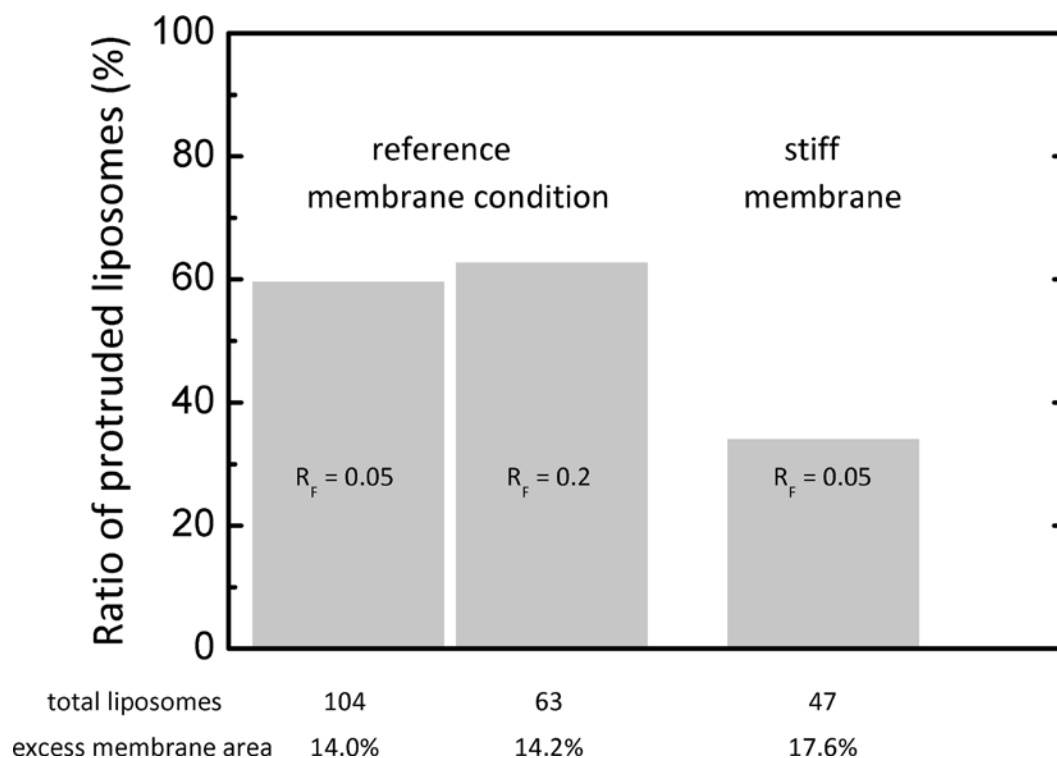


**FIGURE S6** Membrane bending rigidity affects the likelihood of membrane protrusion formation. In all cases, the membranes are floppy with an estimated excess membrane area of 14-17%. At the *stiff membrane* condition, the membrane is decorated with neutravidin.

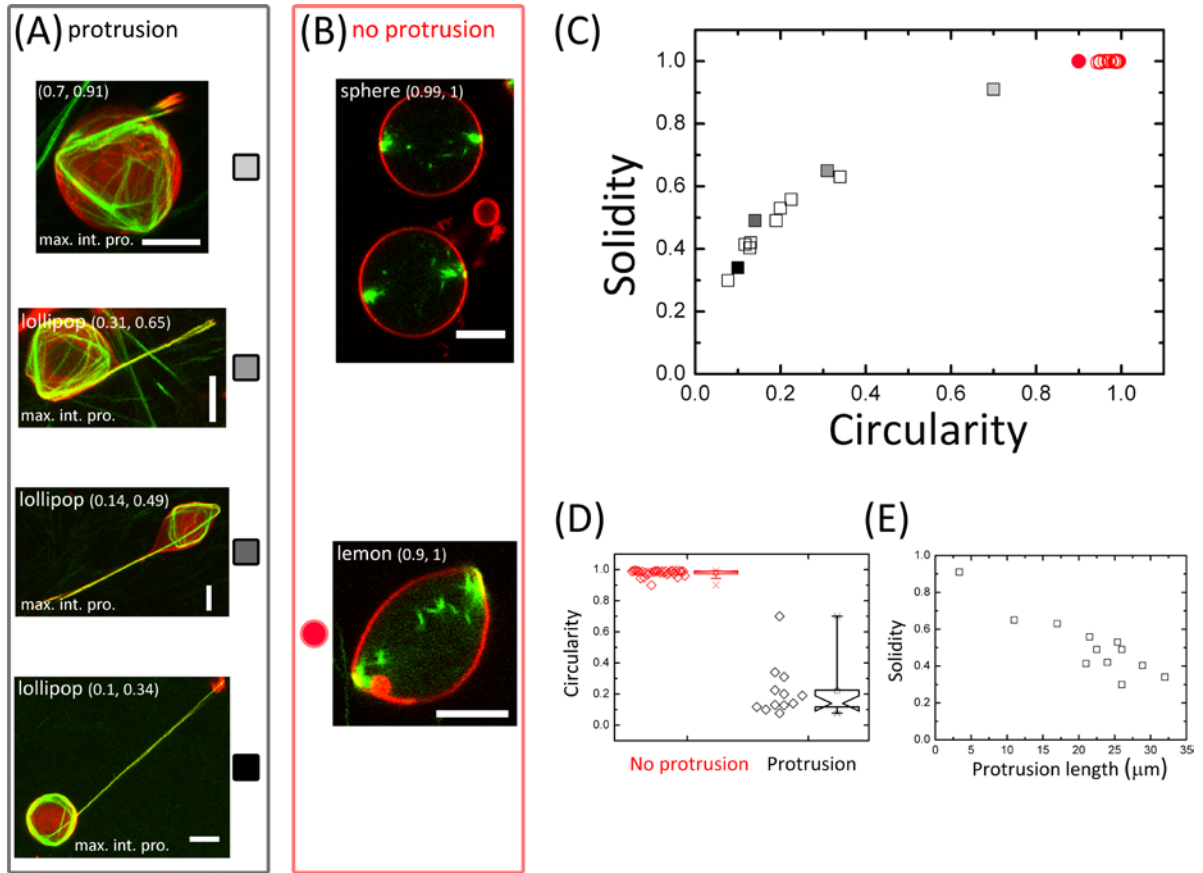


**FIGURE S7** Morphological characterization of a population of 43 liposomes encapsulating actin-fascin bundles ( $R_F = 0.05$ ) at the *stiff membrane* condition, where neutravidin molecules are bound to the liposome membrane via biotinylated lipids. (A and B) Confocal images of liposomes that are increasingly deformed (*top* to *bottom*). In (A), maximum intensity projections (*max. int. pro.*) of confocal sections of liposomes are shown where the number of planes ( $p$ ) over a total  $z$ -range ( $z$ , in  $\mu\text{m}$ ) are ( $p = 30$ ,  $z = 14.5$ ), ( $p = 17$ ,  $z = 8$ ), ( $p = 19$ ,  $z = 9$ ), ( $p = 24$ ,  $z = 11.5$ ) from *top* to *bottom*. In (B), images are confocal sections recorded at the equatorial plane of the liposomes. Red: membrane, green: actin. Scale bars:  $5 \mu\text{m}$ . (C) Liposome shapes are summarized in terms of circularity and solidity. Reddish symbols represent liposomes having no protrusion (31 liposomes) and black/grayish symbols represent liposomes with one protrusion (12 liposomes). Color-coded solid symbols correspond to images of liposomes in (A) and (B). (D) Circularities of liposomes with and without protrusions. (E) The solidity is inversely correlated with the protrusion length (correlation coefficient =  $-0.9057$ ,  $p < 0.001$ ).

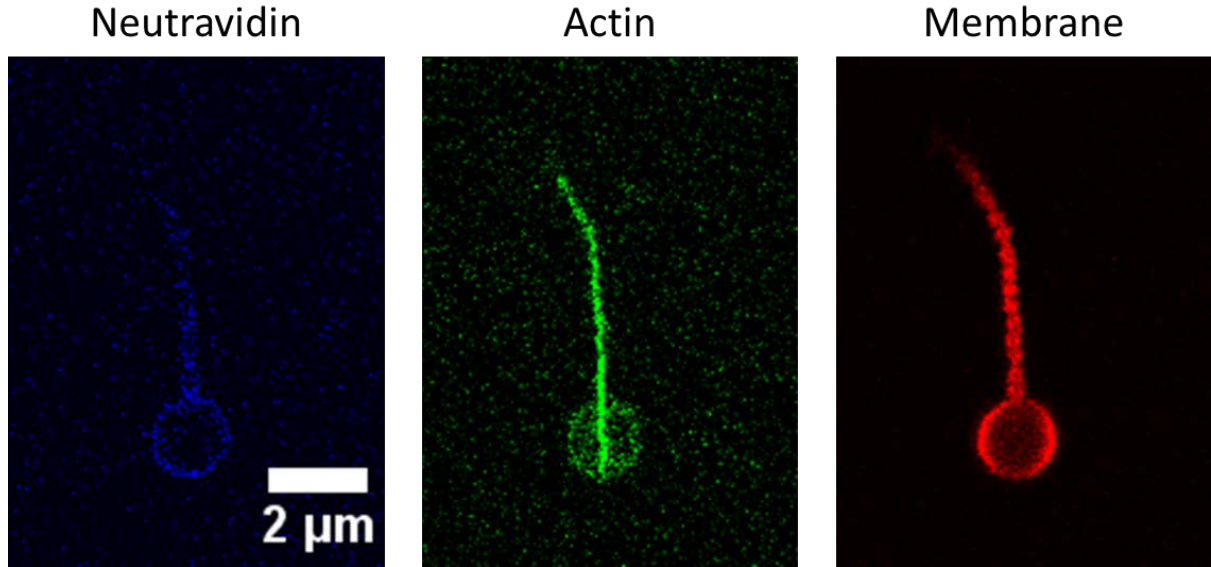


**FIGURE S8** Liposomes encapsulating actin-fascin bundles formed at the *stiff membrane* condition, obtained by decorating the membrane with Alexa350-labelled neutravidin. The neutravidin signal (*left*) co-localizes with the membrane signal (*right*) along the liposome main body and protrusion.

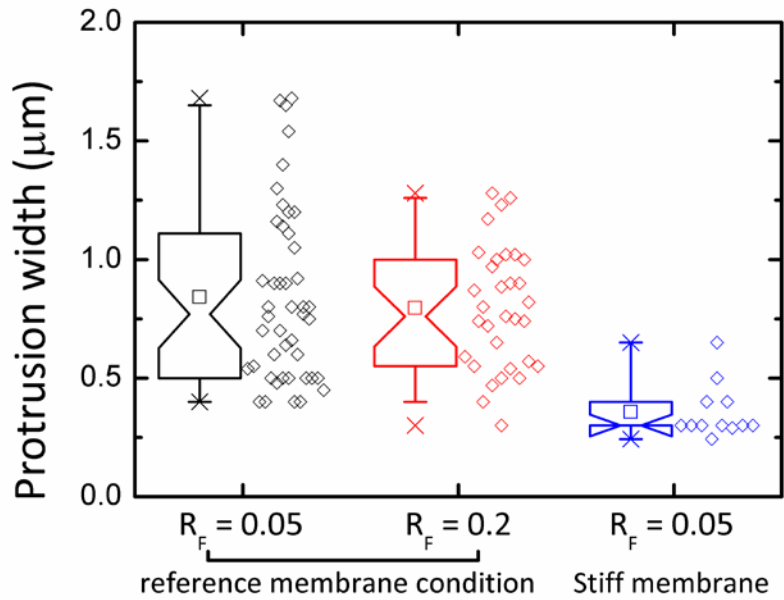
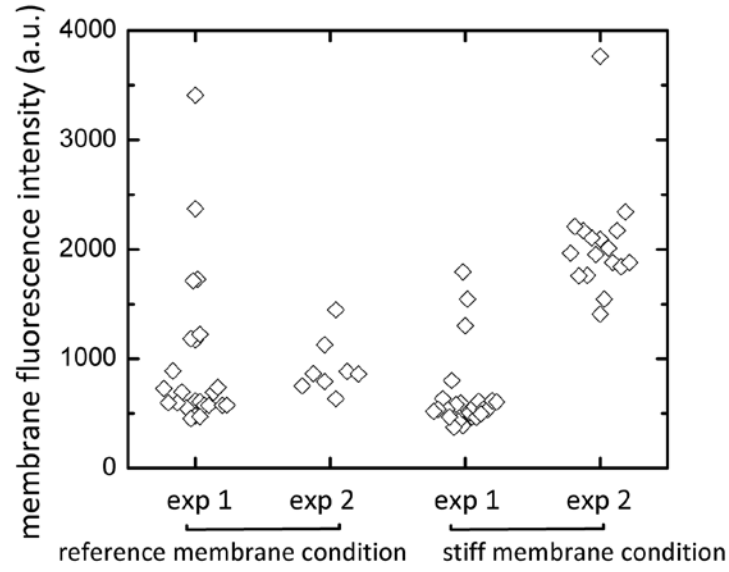


**FIGURE S9** Influence of actin bundle stiffness (modulated by  $R_F$ ) and membrane stiffness (modulated by decorating the membrane with neutravidin) on liposome protrusion width. Liposome population sizes from left to right: 45, 32 and 12.



(A)



(B)

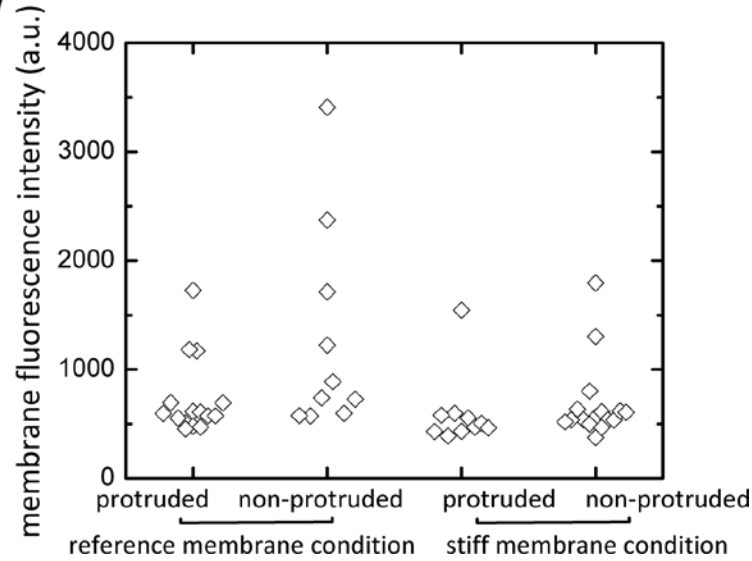


**FIGURE S10** Test of membrane lamellarity distribution. (A) Membrane fluorescence intensities of liposomes at the *reference membrane* condition and at the *stiff membrane* condition. We note that the membrane image corresponding to the data point that has the highest membrane fluorescence intensity value in *exp2* at the *stiff membrane* condition has a few pixels having fluorescence intensity values exceeding the pixel bit depth. Liposome population sizes from *left to right*: 25, 8, 26, 17. (B) Membrane fluorescence intensities of liposomes with and without protrusions obtained in *exp1* at the *reference membrane* condition and at the *stiff membrane* condition. Liposome population sizes from *left to right*: 15, 10, 10, 16. There is no correlation between membrane fluorescence intensity (i.e. lamellarity) and the likelihood of membrane protrusions.

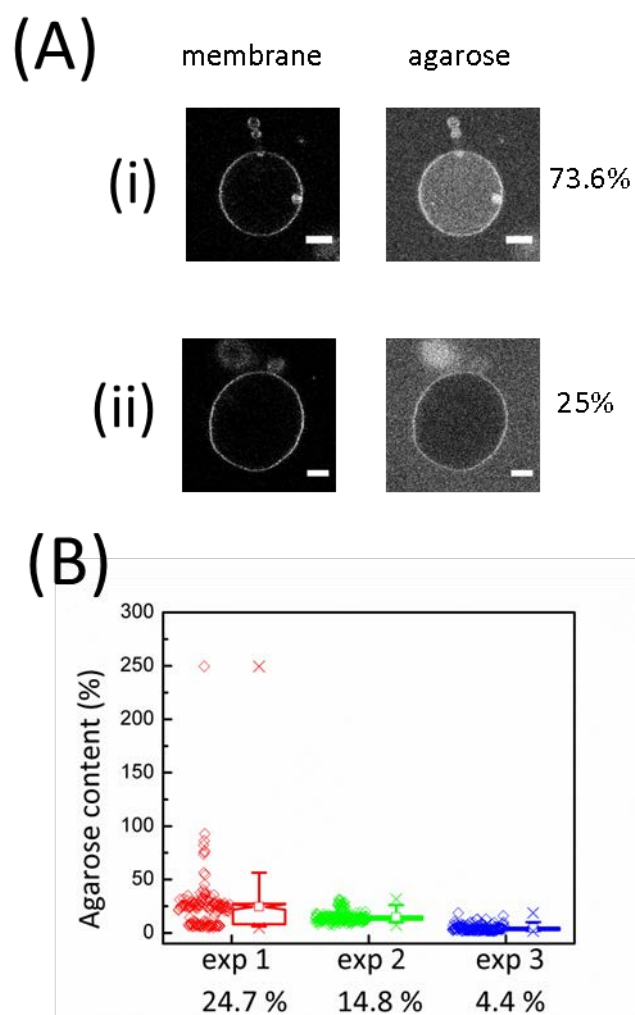


**FIGURE S11** Agarose content in liposomes, quantified by the fraction of a 1% (w/w) agarose solution that remains inside the liposomes after formation. (A) Confocal fluorescence images of two liposomes, (i) and (ii). *Left*: fluorescence signals of liposome membranes. *Right*: fluorescence signals of fluorescently labelled agarose. (B) Agarose content in liposomes with population sizes from left to right: 145, 187 and 156. The average value of agarose content in each experiment is indicated below the graph. Note that in one liposome the agarose content is 250%, indicating a high concentration of agarose inside the liposome, perhaps due to a crowding phenomenon.

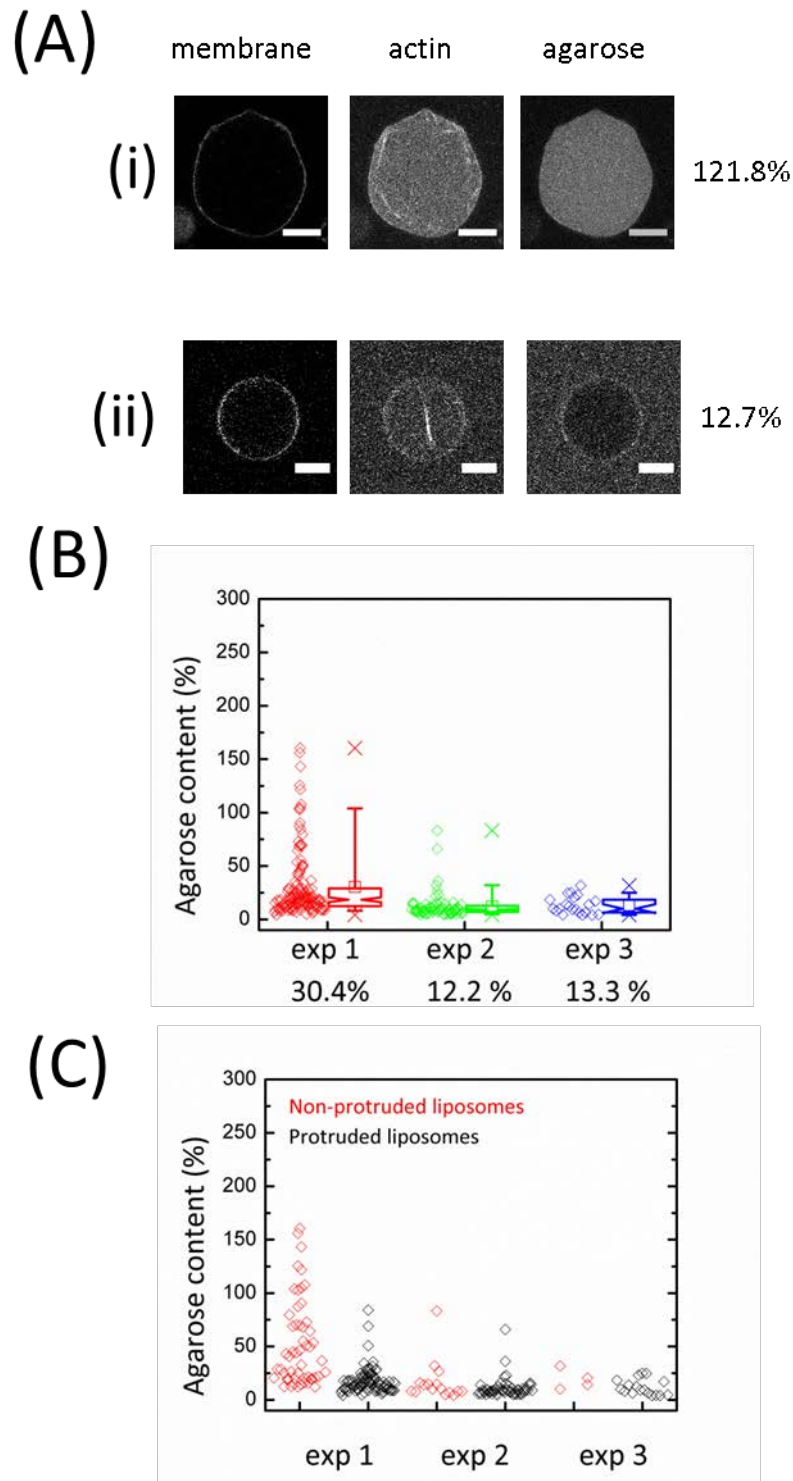


**FIGURE S12** Agarose content in liposomes encapsulating actin-fascin bundles, quantified by the fraction of a 1% (w/w) agarose solution that remains inside the liposomes after formation. (A) Confocal fluorescence images of two liposomes, (i) and (ii), and their corresponding agarose content. In (B), the average value of agarose content in each experiment is indicated below the graph. In (C), for each experiment, the agarose content of liposomes with and without protrusions is shown separately. Liposome population sizes from left to right: (B) 143, 72 and 21, (C) 53, 90, 16, 56, 4 and 17.

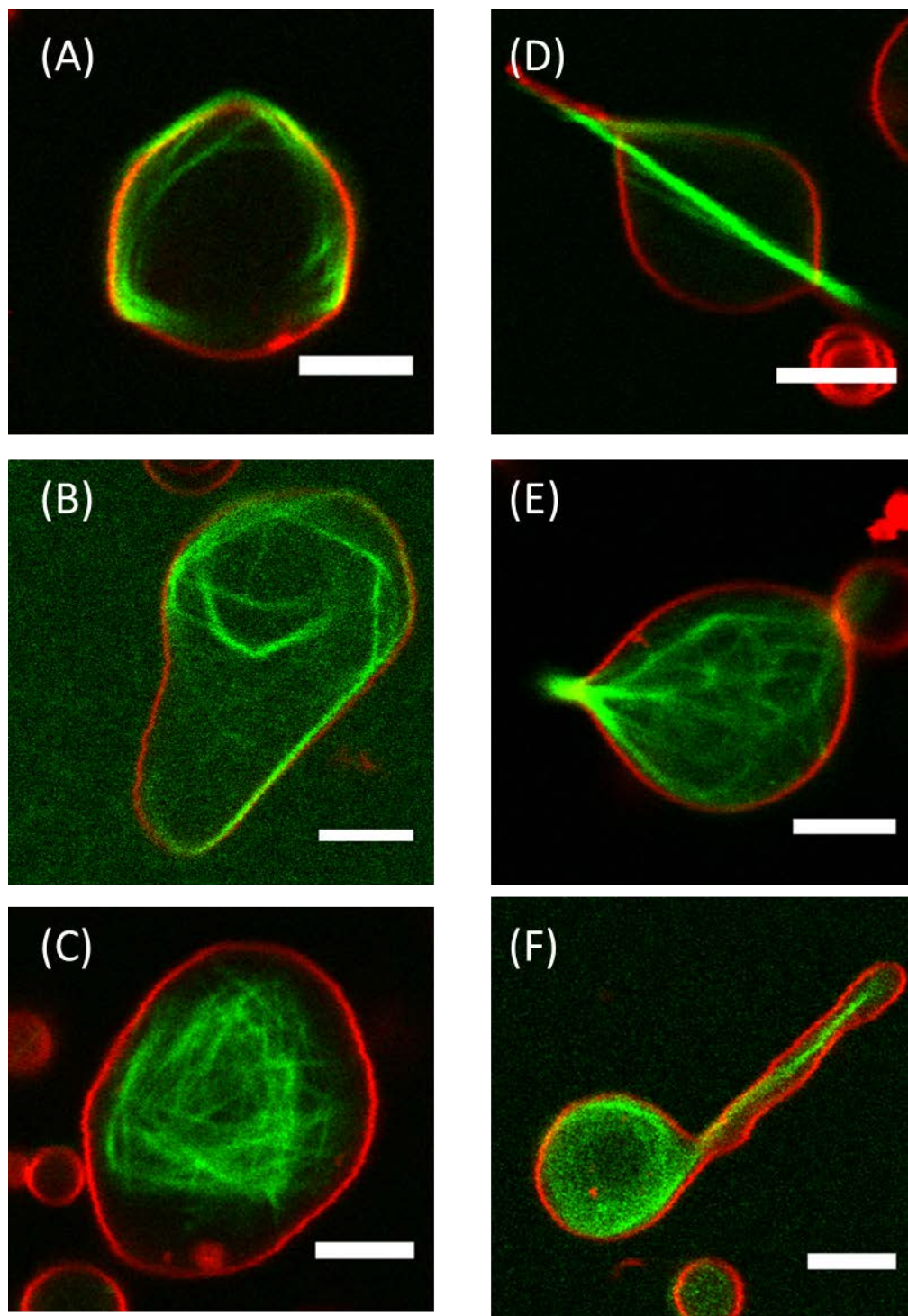


**FIGURE S13** Confocal fluorescence images of PVA-formed liposomes encapsulating actin-fascin bundles ( $R_F = 0.05$ ). Similar to agarose-formed liposomes, we observe a range of morphologies, from non-protruded, to lemon-like, and protruded. Red: membrane, green: actin. Scale bars: 5  $\mu\text{m}$ .

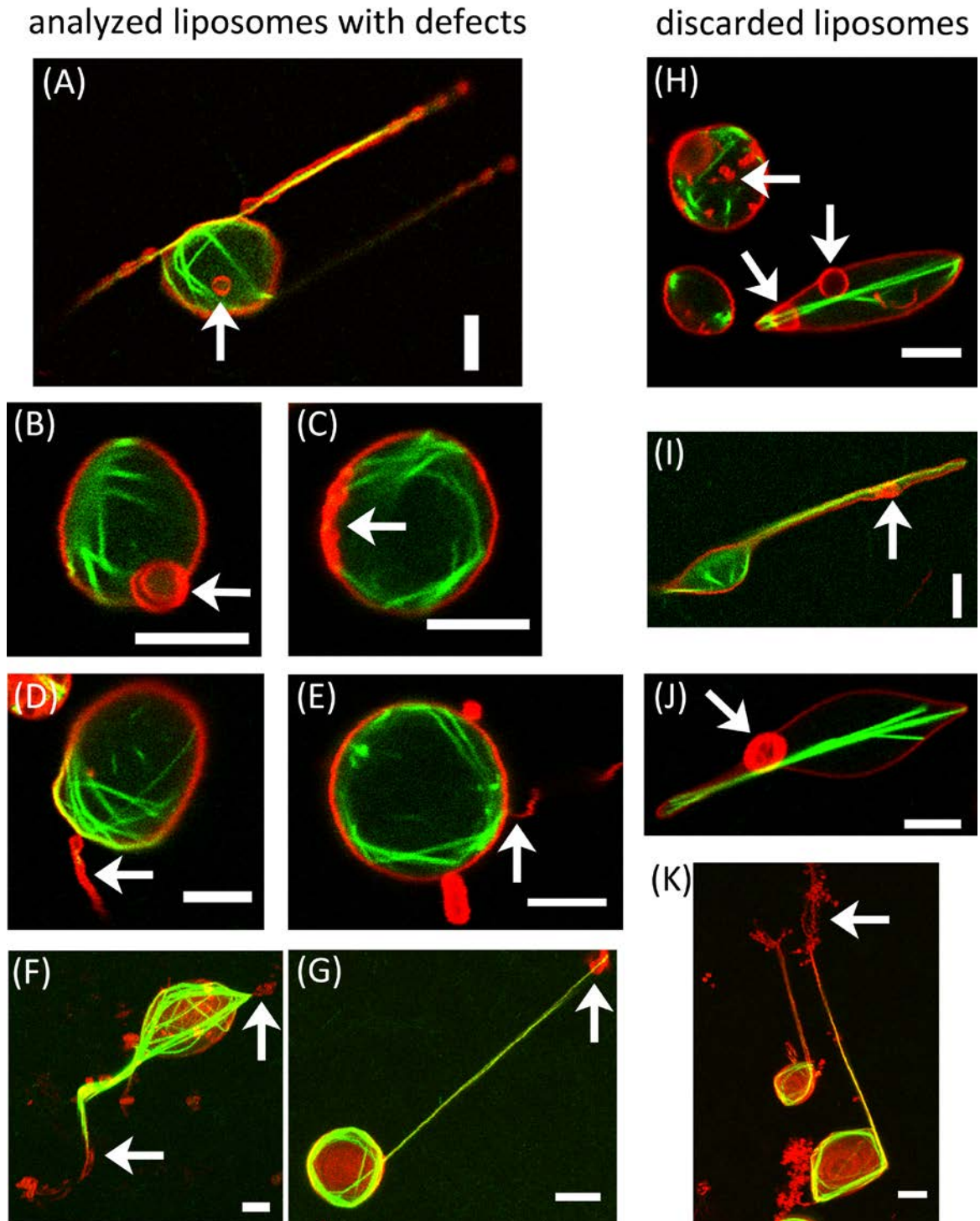


**FIGURE S14** (A-G) Confocal fluorescence images of liposomes having defects that are deemed sufficiently minor to include in the morphological analysis (around 5% of a total of 70 liposomes at the *reference membrane* condition). Defects included: (A) a smaller liposome inside a larger liposome, (B and C) smaller liposomes adhered to the inside of liposome main bodies, (D and E) membrane tubes adhered to liposome membranes, and (F and G) membrane aggregations or tubes adhered to the end of a protrusion or to the main body of liposomes. (H-K) Confocal fluorescence images of liposomes that are discarded from the analysis because membrane shape and/or actin organization are potentially affected by the encapsulated membrane tubes or aggregates, as indicated by the white arrows (around 30% of a total of 70 liposomes at the *reference membrane* condition). Images are single confocal

sections recorded at the equatorial plane of the liposomes, except for (*F*), (*G*) and (*K*), where maximum intensity projections are assembled from 31 planes over a total z-range of 15  $\mu\text{m}$  in (*F*), 24 planes over a total z-range of 11.5  $\mu\text{m}$  in (*G*) and 20 planes over a total z-range of 9.5  $\mu\text{m}$  in (*K*). Red: membrane, green: actin. Scale bars: 5  $\mu\text{m}$ .